Mitchell, Antony J. and Simmons, Kathy and Hann, David B. (2015) Experimental investigation into droplet impingement upon moving films using high speed video and thermal imaging. In: ASME 2015 International Mechanical Engineering Congress & Exposition (IMECE 2015), 13-19 Nov 2015, Houston, Texas, USA.

Proceedings of the ASME 2015 International Mechanical Engineering Congress & Exposition
IMECE2015
November 13th - 19th, 2015, Houston, USA

IMECE2015-51677

EXPERIMENTAL INVESTIGATION INTO DROPLET IMPINGEMENT UPON MOVING FILMS USING HIGH SPEED VIDEO AND THERMAL IMAGING

Antony J. Mitchell
Technology Centre for Gas Turbine Tranmsission Systems,
The University of Nottingham,
Nottingham, NG7 2RD, UK

Kathy Simmons
Technology Centre for Gas Turbine Tranmsission Systems,
The University of Nottingham,
Nottingham, NG7 2RD, UK

David Hann
Technology Centre for Gas Turbine Tranmsission Systems,
The University of Nottingham,
Nottingham, NG7 2RD, UK

ABSTRACT

Aeroengine bearing chambers are geometrically complex, typically containing shafts, bearings, seals and stationary components. Oil is supplied for lubrication and cooling and so the chamber contains a highly rotating two-phase (oil/air) flow where the oil is typically present as droplets, ligaments, mist and films. These films may be thick or thin and film speed varies with chamber location. It is desirable to know *a priori* the outcome of a droplet-film impact event in terms of mass, momentum and energy transfer.

There is a significant body of research on the interaction between droplets and static films. The experimental parameter space has been characterised on the basis of film thickness and impact parameter to predict the outcome of an impingement. The impingement of droplets on moving films has only begun to be investigated over the last decade and consequently models have not yet been developed and the parameter space has barely begun to be characterised.

Within this paper results are presented from an experimental study in which water droplets of 3 mm and 3.8 mm at $20°C$ falling under the influence of gravity impinged onto water films flowing down an inclined plane. Film temperature was $30°C$ and film thicknesses were between 2.3 mm and 4.2 mm. High speed imaging was used to determine the impingement outcomes and cavity morphology. A high speed infrared camera was used to determine the extent of the thermally affected region and its temperature behaviour.

We find that by using the resultant droplet velocity (combining droplet and film velocities) the film impingement outcomes can be characterised into regions very similar to those for static films. The data is presented as a function of splashing parameter and non-dimensional film thickness. It was observed that for these impacts on supercritical films ($\mathrm{Fr} > 1$) there is less propensity for secondary droplet formation through jet breakup than on static and subcritical films ($\mathrm{Fr} < 1$).

Data was obtained for extent of the thermally affected region. It was found that the cooler droplet liquid spreads over the inside of the crater before heating up to film temperature. Development of crater shape and size was also studied and data compared to established models for droplet impact on deep static films. During the initial stages of an impact crater area increases similarly to that for static films although the crater shape itself is less similar and is asymmetrical due to the film motion.

INTRODUCTION

The interaction between droplets and moving films is a remarkably common occurrence, from simple environmental effects such as raindrops upon a river to the field of interest here, the complexity of an aeroengine bearing chamber. Aeroengine bearing chambers are sealed regions within an aeroengine housing the bearings that locate and support the rotating shafts. Oil is supplied to the bearings for lubrication and cooling and this oil is typically present in the form of droplets, ligaments, mist and films creating a complex and highly rotating multiphase flow of air and oil. The oil temperature varies around the system and

where droplets impact on surface films the droplet will usually be at a different temperature from the film. When it comes to characterising the outcome from a droplet-film impact event it transpires that although there is a significant body of experimental literature covering droplet impacts onto static films there is very little published for impacts onto moving films. A study by Alghoul et al [1] for droplets impinging almost normally onto a subcritical film (film with Froude number less than 1) showed that the impingement outcomes and crater morphologies were subtly changed/distorted compared to impact on a static film.

The work presented in this paper aims to investigate how impingements upon thinner, faster supercritical films (Froude number greater than 1) compare to established static film data, and where appropriate devise models and correlations for these behaviours.

REVIEW OF PREVIOUS WORK

Although investigations into droplet impingement upon liquids can be traced back to 1908 [2], the majority of research into this topic has been conducted upon stationary films, and these situations can vary significantly from an impingement onto a moving film. This section provides an overview of key previous work that has been undertaken regarding droplet impingement onto both static and moving films.

Normal Impingement upon Static Films

In modern times, investigations into droplet impact dynamics have been undertaken by many researchers with key publications from Coghe at al [3], Cossali et al [4], Rein [5], Manzello & Yang/Manzello et al [6–9], Rioboo et al [10] and Okawa et al [11].

These papers identify four possible regimes resulting from droplet impingement on a static film: *floating*, *bouncing*, *coalescence* and *splashing*. *Floating* is observed when the kinetic energy of the droplet is small enough that it doesn't break the gas layer between the droplet and the film so that the droplet remains above the film and separate from it. If the kinetic energy is increased, it is then possible to observe the droplet *bouncing* off the surface of the liquid. A further increase in kinetic energy will cause the droplet to break through the gas layer, causing it to *coalesce* with the film. This typically involves the formation of a crater at the impact location with the possibility of a rim forming around the edge of the crater, and sometimes a jet of water protruding upwards, formed when the crater collapses in upon itself. Finally, further increasing the droplet's kinetic energy results in *splashing*, defined ([4], [12], [13]) as where secondary droplets are formed either from the rim of the crater, (*crown splashing*), or from the central jet (*jet breakup*).

Cossali et al [4] observed a type of splashing they termed *prompt* splashing during some water-water impact events. *Prompt* splashing is usually associated with droplet impact onto dry, rough surfaces and is where droplets form immediately at the impact event. It is far more common for impact to initially result in a crown that subsequently breaks into droplets. In [4] it was noted that the droplets produced were typically much smaller and with higher velocity than those produced from crown splashing. It was also postulated that the energy threshold for *prompt* splashing may be lower than that for *crown* splashing.

Vander Wal et al [14] also observed *prompt* splashing in the course of their experiments. This was described as being associated with the advancing crown, rather than with the crown receding, which was identified as the cause of *crown* splashing. It was found that for non-dimensional film thicknes $1 \leq \delta \leq 10$ the liquid film inhibited prompt splashing, causing it to be minimal compared to films of $\delta \leq 1$. By all accounts, the volume of fluid ejected following an impact event is inconsequential for *prompt* splashing compared to the volume entrained within the air by crown splashing and jet breakup. It was found that *prompt* splashing was affected by the surface tension and viscosity of the fluids used in the experiment.

Controlling dimensionless Parameters

Throughout the published literature, various dimensionless parameters are used, The most basic of these are Reynolds Number (Re), Weber Number (We), and Ohnesorge Number (Oh). Film thickness is also commonly non-dimensionalised by droplet diameter as δ.

Cossali et al [4] defined thick films as where $\delta > 1$ and thin films as where $\delta < 1$. This is important, as thick films tend towards jetting behaviours [1, 9, 15], whilst thin films tend towards crowning behaviours [4, 10, 16–18].

Attempts have been made to correlate impingement outcomes using the droplet Weber number. Cossali et al [4] determined the critical We for combinations of film thickness and Oh. Manzello & Yang [9] found the critical We for transition between jetting and jet breakup on static films to be $We = 74$. However, perhaps the most important dimensionless parameter in the field of droplet impingement is the *splashing parameter*, K. This is variously defined. Mundo et al [19] have

$$K_{Mundo} = Oh\, Re^{1.25} \tag{1}$$

Cossali et al [4] use

$$K_{Cossali} = Oh\, We^{-0.4} \tag{2}$$

and Huang & Zhang [20] prefer

$$K_{Huang} = Re^{0.25}\, We^{0.375}. \tag{3}$$

TABLE 1: TRANSITION VALUES OF $K = We\ Oh^{-0.4}$

Behaviour boundary	Transition value of K	film thickness range	Reference source
No crown/ crown	400	$0.06 < \delta < 0.015$	[10]
No crown/ crown	700	$0.5 < \delta < 2$	[11]
Crown/ crown splash	2100	$0.06 < \delta < 0.015$	[10]
Crown/ crown splash	2100	$0.5 < \delta < 2$	[11]
Crown/ crown splash	$2100 + 5880\delta^{0.23}$	$0.1 < \delta < 0.2$	[4]
Crown/ crown splash	$2074 + 870\delta^{0.23}$	$0.1 < \delta < 1$	[21]
Jet/ Jet breakup	8000	$0.6 < \delta$	[3]

Of these various definitions, $K_{Cossali}$ is the most prevalent in the published literature, with some of the key transition regimes being established by Tropea & Marengo [21], Okawa et al [11] and Rioboo et al [10]. Table 1 details these identified transitions for droplets impinging on static liquid films.

Oblique Impingement upon Static Films

Okawa et al [22] investigated the impingement of droplets onto a static film with impingement angles α, (see Fig. 1 for definition of angle) between 11 $^\circ$ and 75°. This case is somewhat similar to near-normal impact on a moving film in that there is relative horizontal motion between the droplet and film and therefore similarities might be expected between the behaviours. It was found that for these non-normal impacts, using the total droplet velocity (v_d), rather than the normal velocity (v_n), as illustrated in Fig. 1, caused the transitions to correlate with those established for normal droplet impingement. Furthermore, it was found the crown formation was asymmetrical, in an oblique impact, with the crown tending in the same direction as the droplet was travelling. The angle of the impact caused distinct variances in the mass of material ejected from the crown in the form of droplets.

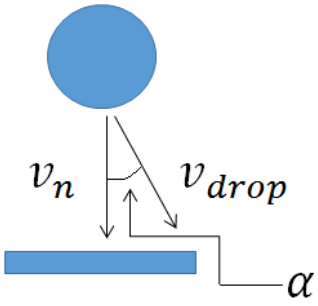

FIGURE 1: Illustrating the velocity v_d used by Okawa et al [22] to calculate the impact parameter for non-normal impingements on static films

Impingement upon moving Films

Alghoul et al [1] investigated normal droplet impingement on sub-critical moving films. It was observed that the craters formed after impact were not initially symmetrical but that they became more symmetrical with time, eventually forming a cone with a sharp point before collapsing inwards. It was also observed that the centre of the crater moved downstream with time, travelling with the film. In an impingement scenario with crown formation, it was observed that the crown was higher on the upstream side of the crater than the downstream side. Where jets were formed, it was observed that they did not form normal to the film, but tended to angle downstream. The height of the jet was found to depend on the film thickness, in keeping with the findings of Macklin & Hobbs [15] for droplet impact on static films. However, the observations with regard to jet height did not follow the findings of Manzello & Yang [9] for static films, as the jet height did not begin to level off after the film thickness was increased above 7mm. Alghoul et al attributed this behaviour to the movement of the film.

Established Models for Crater Morphology

Although less attention has been paid to the sub-surface phenomena of droplet impingement, investigations have still been undertaken. An early paper was written by Macklin & Hobbs in 1969 [15] and this stated that for droplets of 2.3 mm impinging at 3.2 m/s the formation of the subsurface cavity did not differ for depths of water between 20 mm and 10 mm. However for films of 6 mm deep ($\delta = 2.61$) the crater propagation began to slow with time as the cavity neared the rigid base. And when the depth was less than 9 mm ($\delta = 3.91$) a slight flattening of the base of the cavity was observed. Finally, for film heights of below 6 mm, the cavity was found to puncture completely through the liquid, to the bottom of the container.

The key papers that have produced models for crater forma-

tion following droplet impingement are Berberovic et al [23] and Bisighini et al [24] for droplets on static films, and Lagubeau et al [25], for droplets on solid substrates.

Berberovic et al [23] and Bisighini et al [24] investigated crater propagation for droplets impinging onto very thick static films. From their work Berberovic et al derived equations representing crater formation, and undertook numerical modelling (using computational fluid dynamics) using these to create models for static impacts. The numerical data was compared against experimental data. However this approach is quite complicated as it includes CFD calculations. Fortunately Bisigini et al created a model that can determine the correlation using only the key parameters of the droplet in a differential equation. In this current work the experimental data obtained is compared to the correlation of Bisighini et al. This model uses a series of differential equations to derive a curve for the crater diameter at different nondimensional timesteps from the initial droplet parameters.

Lagubeau et al [25] investigated droplet impingements onto solid surfaces. From this an equation for the minimum thickness of the droplet material was derived. It is hypothesised that this same minimum thickness of droplet material will be found when a droplet impacts on a thin film and spreads out over the film surface and this will be investigated in future analysis of current data.

EXPERIMENTAL SET UP

This section outlines the test facility and equipment used to perform the experiments, including an the method of droplet production and the methodology of data acquisition.

Testing Apparatus

The apparatus used for the experiment is shown schematically in Fig. 2 with a photograph of the droplet impact region in Fig. 3.

The facility consists of an inclined channel along which the water film flows fed from a header tank. The water is heated above ambient temperature in the water tank, which is fitted with a PID controlled heating element (*Watlow EZ Zone* PID controller and *Redring 33324601* heating element) to ensure a constant water temperature (typically, 30°C). The water is pumped using a *Nocchi Pura Dom* pump through a $50\mu m$ filter to the header tank and a constant pressure head is achieved by using an overflow in the header tank that returns water to the main tank. From the header tank water flows through a control valve and a flowmeter (*RS components 441-4879 Liquid Flow Indicator*) to the perspex channel, which is 1400 mm long by 50 mm wide.

Film thickness

The perspex channel was inclined at 10° to the horizontal and liquid flowrates in the range 4 to 12 litres per minute were used. For an inclined channel flow the film height and volume flowrate are not independent once fully developed flow is achieved. Prior to the main tests, measurements were taken at distances along the channel to establish that fully developed flow exists for each flowrate by the point of droplet impact. During testing the thickness of the film in the channel just upstream of droplet impact was obtained using a Keyence LT-9030M sensor mounted on a micrometer. The Keyence sensor outputs data as an analogue signal in the range of $-10V$ to $+10V$ based on the distance. This signal was recorded using a National Instruments USB-6009 DAQ before being combined with the micrometer reading and converted to a film height using a MATLAB script.

Droplet Production

Droplets were produced using a Nordson EFD Ultimus air-powered fluid dispenser commonly used to dispense precise amounts of fluid in medical applications. This dispenser uses a solenoid to allow precise amounts of pressurised gas into a syringe, forcing water out of the end of a needle. This was then tuned by changing the gas pressure using the inbuilt regulator, and by varying the amount of time the solenoid valve was open for to be create droplets of consistent diameters throughout testing. Data was obtained for two droplet sizes: 3.0 mm $\pm$ 0.3 mm and 3.8 mm $\pm$ 0.3 mm. Droplets were released from two heights (0.2 m and 0.35 m, falling vertically under the influence of gravity to give two impact velocities. For these experiments the droplets were water at ambient temperature (ie below the film temperature).

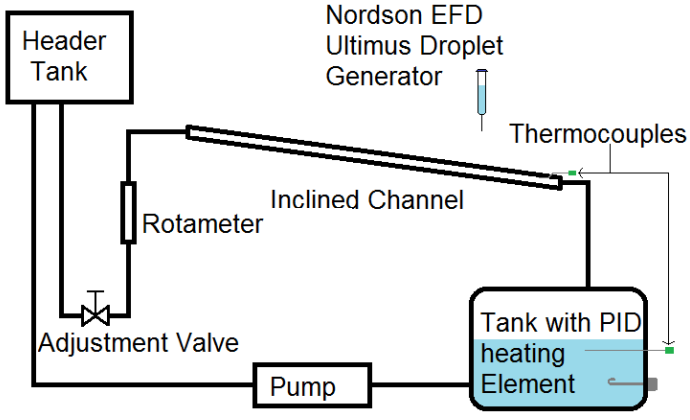

FIGURE 2: Schematic diagram of the experimental test rig

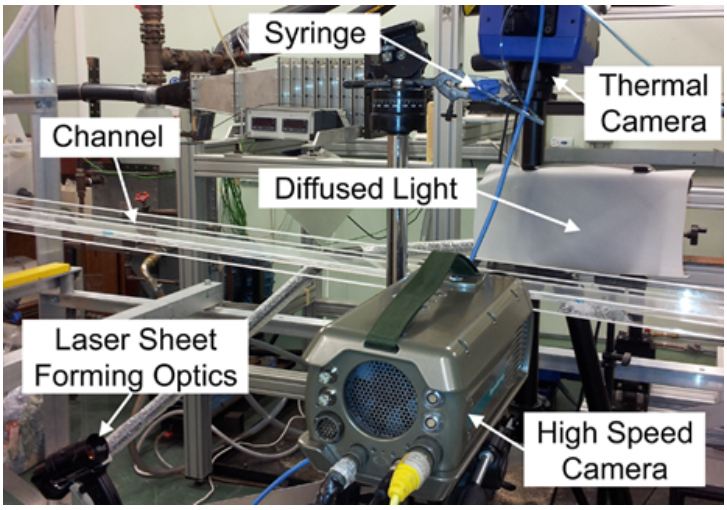

FIGURE 3: **Photo of the experimental test rig showing the positioning of the infrared and high speed cameras, lighting and droplet generator**

Data Acquisition

Images of each droplet impact event were recorded using a high speed camera looking from the side of the channel and a thermal imaging system looking from the top of the channel as can be seen in Fig. 3. The high speed camera used is a *Phantom V12.1* high speed camera, this was set to record images with a resolution of 1280×800 pixels at $600Hz$ and a short exposure time of $100\mu s$ to avoid motion blur upon the droplets. The lens was a Nikon Micro-NIKKOR 105mm f/2.8 AI-s. The infrared images were acquired using a *FLIR SC7000* recording at $300Hz$.

DATA PROCESSING

This section details the post-processing applied to the data, the analysis of the data to determine key characteristics, and the production of graphs and charts.

High Speed Camera Data

Prior to obtaining the impact event sequence of images a calibration image was obtained using a calibration target and this was used to determine the scaling factor of the image in *mm/pixel*.

For the impact event image analysis a MATLAB program was written and applied. The first step of image processing for the high speed camera data was to correct for uneven illumination using some of MATLAB's morphological operations. For each image the contrast was maximised using the *imadjust* function. In each image the droplet was detected using canny edge detection and the function *imfindcircles*. Multiple frames were

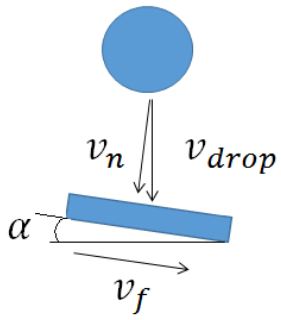

FIGURE 4: **Illustrating the velocity components from which the magnitude of resultant velocity is obtained**

compared to determine the average droplet radius and the velocity of the droplet. This information allowed *We*, *Oh*, *Re* and $K_{Cossali}$ to be calculated.

The Cossali splashing parameter $K_{Cossali}$ was calculated using the magnitude of resultant velocity formed by combining the droplet velocity and the film velocity. For oblique impacts on static films Okawa et al [22] found the actual droplet velocity gave the better correlation than the normal component. Here, having plotted the data using normal, droplet and resultant velocity magnitudes in $K_{Cossali}$ it was concluded that the resultant was the better choice in terms of equivalence to data for normal droplet impact on static film.

Fig 4 illustrates the droplet velocity v_d and the component normal to the film v_n.

For each image sequence the impingement outcome was categorised into one of *coalescence*, *crown formation* (without splashing), *crown splashing*, *crown splash with jetting* (no jet breakup) and *crown splash with jet breakup*. Example images for each of these outcome types is given in Fig. 5.

This data is shown in Fig. 6 where splashing parameter $K_{Cossali}$ is on the y-axis of the chart and non-dimensional film thickness on the x-axis. Also included on this graph are the lines representing the transitions identified in Table 1. The line delineating crown formation from crown splashing as found by Tropea & Marengo [21] has been here projected to higher non-dimensional film thicknesses.

Infrared Camera Data

An infrared camera is sensitive to electromagnetic radiation in the infrared spectrum. Infrared radiation is emitted by all bodies with a temperature above absolute zero and in simple terms the amount of radiation increases with the temperature of the body and thus the amount of infrared radiation detected corresponds (once suitably calibrated) to the surface temperature. Infrared data is usually presented using pseudo-color images, where the color is used to represent the assigned temperature

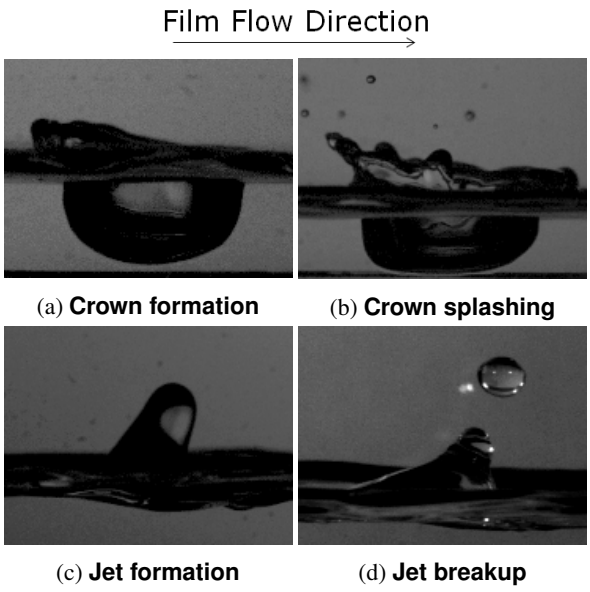

FIGURE 5: **Splashing regimes on moving films**

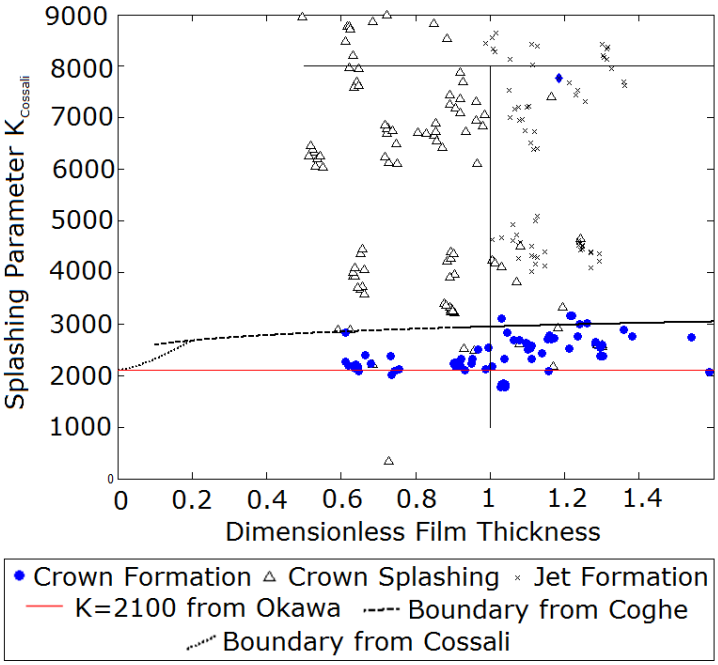

FIGURE 6: **Splashing parameter K against δ (using magnitude of resultant velocity) and showing some of the key transition boundaries for static films**

value. The surface infrared data captured by the thermal imaging system in this study therefore gives a measure of the temperature of the film surface before and during a droplet impact event. As the droplets are cooler than the film, it is possible to see the region over which the film surface temperature is modified by the presence of the droplet.

During a droplet film impact event the droplet liquid spreads out over the film and heat transfer/mixing takes place. Initially on a thermal image the droplet can be clearly seen due to the temperature difference but as mixing and heat transfer take place the film surface returns to a single temperature. In these experiments where single droplet impact events are investigated the final film temperature is indistinguishable from that before droplet impact. The infrared thermal images are used to track the temperature of the droplet impact zone during the impact event. Images from the infrared camera were imported into MATLAB where the digital brightness scale was converted into temperature using a previously obtained temperature calibration curve. A typical infrared image is shown in Fig. 7 alongside the matching image from the high speed camera.

It is worth commenting that an infrared image does not show the location of the droplet liquid during the impact event. In work not yet published we have used fluorescent dye in the droplet liquid and to some extent this allows us to tract where the droplet liquid goes during the impact process. With the thermal imaging we are following the thermal energy, which can of course move (primarily through conduction in this case) without convection. Thus film fluid adjacent to cooler droplet fluid will become cooler through energy transfer.

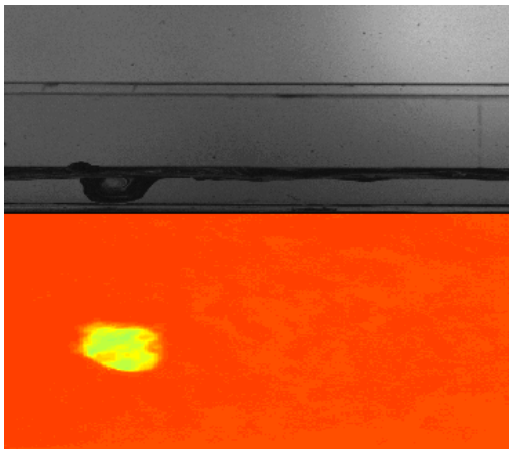

FIGURE 7: **A typical image pair, high speed camera image above and infrared camera image below. Film travelling left to right**

To determine the size and temperature of the droplet impact thermal region the image is thresholded. This was done using

logical operators in MATLAB, by determining the temperature mean ($\bar{T}$) and standard deviation (σ_T) across the entire image and then setting a threshold using:

$$T_{Threshold} = \bar{T} - [3\sigma_T]. \quad (4)$$

Using 3σ ensured that cool region was detected accurately and that no false values from the film were detected. This binary threshold was then applied to the original image to generate a masked image, where only those pixels below the threshold were present. The number of pixels within this region (giving its area) and its average temperature were then determined.

It was observed that the impact region was slightly oval, compared to circular regions typical of static film impacts. In order to compare the evolution of the size of the impact region with time against the model from Bisighini et al [24] the equivalent radius was calculated from the impact region area. Fig. 9 shows the current crater size evolution data and compares it to that from Bisighini et al [24] for droplet impact onto a static film.

RESULTS AND DISCUSSION

The analysis of a single droplet of water falling vertically onto a supercritical water film travelling on a plane inclined at 10° to the horizontal is presented in this section. Both visual analysis of the impingement outcome and measurements of the crater morphology are included.

Impingement Outcomes

The calculated values of $K_{Cossali}$ and impingement outcomes (qualitative descriptor) are plotted against the dimensionless film thickness (δ) in Fig. 6. For the parameters so far investigated there were no incidents resulting in *coalescence*. Within experimental uncertainty *crown formation* is observed only below the line given by $K_{Cossali} = 2074 + 870\delta^{0.23}$ which is the same upper limit previously found for droplet impact onto static films (see Table 1). However, it is worth noting that the *crown splashing* region extends below this line, overlapping the *crown formation* region.

Further analysis was carried out for these cases where $K_{Cossali}$ falls below the Tropea & Morengo line but splashing was observed. These cases were those for which film speeds were higher and films were thinner and in many of these cases is was more appropriate to categorise the impingement outcome as *prompt* splashing rather than *crown* splashing as no crown was actually formed. Fig. 8 shows the split of *crown* splashing and *prompt* splashing points. This shows that in all cases where there is splashing observed at lower values of impact parameter it is *prompt* splashing.

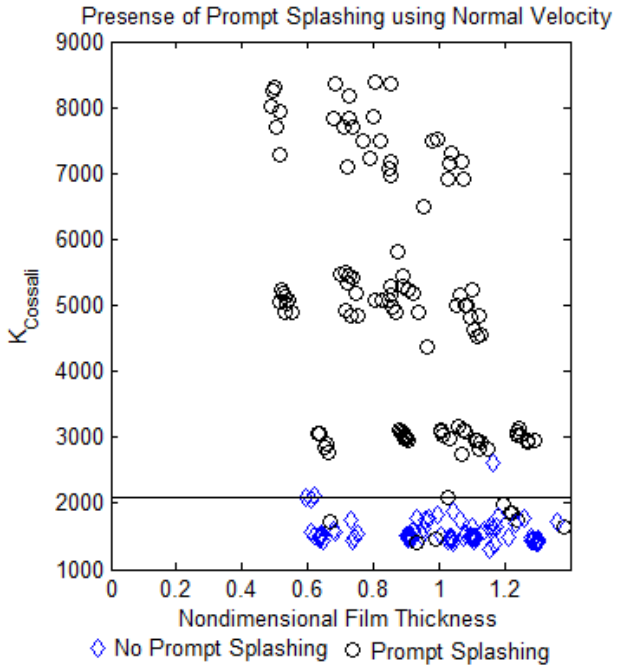

FIGURE 8: **Graph showing which of the impact events are characterised as *prompt splashing*. $K_{Cossali}$ against δ**

For static films crown splashing with jet formation was only observed when $\delta > 1$ and this appears to be the same for the films investigated here. However, for static films the onset of jet formation is at $K_{Cossali} = 2100$ whereas for these supercritical films ($Fr > 1$) the lowest value of $K_{Cossali}$ for which crown jetting is observed is 2700. This corresponds to the findings of Alghoul et al [1] for subcritical films ($Fr < 1$) where this behaviour also was not observed until around $K_{Cossali} = 2700$.

The observed cases of *crown splashing with jet breakup* were all at values of $K_{Cossali}$ and δ where *crown splashing* was observed for other parameter combinations. This may be attributed to disturbances in the film inhibiting jet production but further data analysis will be carried out to confirm this.

As might be anticipated, crown formation and droplet production always tend towards the upstream side of the crater - Fig. 7 illustrates this. This concurs with the findings of Okawa et al [22] and Sikalo et al [26] about crown asymmetry when there is relative velocity between the film and the droplet. Jetting behaviour tended to be in the downstream direction, which is in agreement with the findings from Alghoul et al [1].

For films moving on an inclined plane film velocity and film depth are not independent variables. For Froude number greater than unity (supercritical film), at each flowrate there exists a single film speed and corresponding film depth. Consequently there is some further work required to fully characterise the experi-

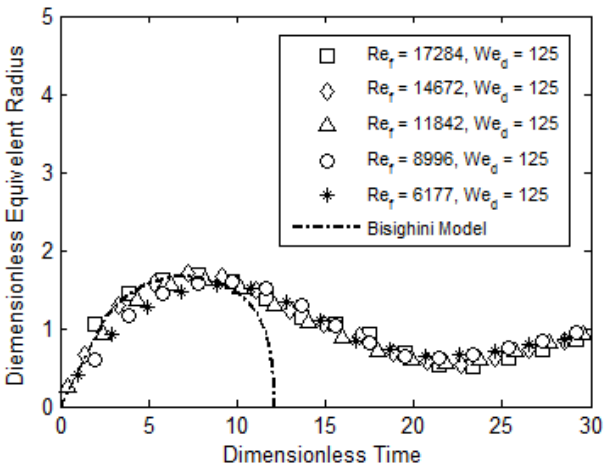

FIGURE 9: **Dimensionless equivalent crater radius against dimensionless time, alongside the model from Bisighini et al [24]**

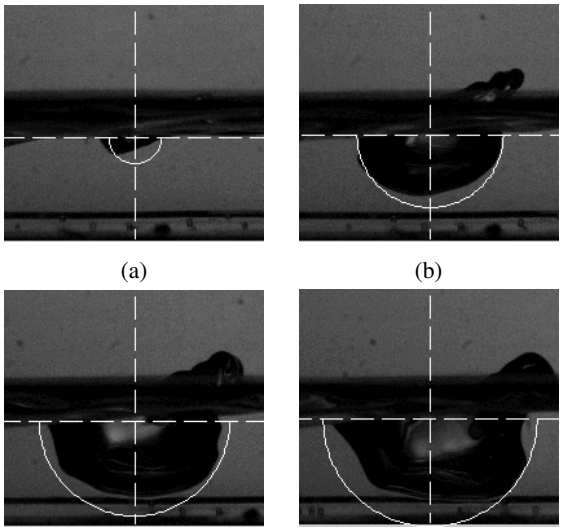

FIGURE 10: **Timeline of droplet impingement for We = 125 and δ = 1.292 in steps of 1/300s. Film flow is right to left here.**

mental space by looking at different plane angles where the film thickness for a given flowrate (and of course film velocity) would be modified.

Crater Morphology

This section investigates the evolution of the crater in terms of size and shape as a function of time. The method chosen for this part of the study was to calculate a crater equivalent radius using area data from the infrared camera images. The area data was obtained using MATLAB and a method analogous to that described for the infrared images. The equivalent radius is non-dimensionalised with droplet diameter, ϕ (measured from the image just before impact). Time is non-dimensionalised as τ following Bisighini et al [24] with the timescale ϕ/v_n.

Fig. 9 shows the dimensionless equivalent radius of the crater plotted against dimensionless time for $We = 125$ and five Reynolds numbers in the range $Re = 6177 - 19284$. The chain dashed line in the figure is obtained from the correlation of Bisighini et al [24] for $We = 125$ and a static film. This figure shows that crater evolution for droplet impact on a moving film shows significant similarities to the static film data up to $\tau = 10$. It is of interest to note that the resultant velocity appears to give better correlation to static film data where impact outcome is concerned but here, for crater evolution, using the resultant velocity over-estimates the crater radius and for this reason normal velocity was used.

Fig. 10 shows four images of crater development in increments of $t = 1/300$. This image is typical of all those obtained. The dashed lines represent the centroid of the crater, and the semicircle is the predicted radius from the model by Bisighini et al [24]. For the first timestep the model underestimates the crater depth and diameter, this is due to the propagation being in the *pressure dominated region* as postulated by Lagubeau et al [25]. In these timesteps, the crater is larger on the downstream side.

The model appears to correlate relatively reasonably well with the crater width through Figs. (10b-10c) but the depth is significantly overestimated by the model. This is due to forces emanating from the bottom of the channel, Macklin & Hobbs [15] observed a flattening of the bottom of the crater at this point, which is similarly seen here, and is responsible for this overestimation of depth. The asymmetry of the crater observed in the earlier steps of propagation is much reduced in these intermediate timesteps as the faster flow of the top of the film gradually overcomes the effect of the droplet impact. Ultimately the film flow leads to assymetry of the crater in the opposite direction as shown in Fig. (10d).

Thermal Effects

The mean temperature of the droplet liquid observed by the infrared camera is shown against time in Fig. 11 where non-dimensional temperature (T^*) is plotted against time.

For each Weber number there are five film Reynolds numbers and although it is clear from Fig. 11 that Reynolds number has an effect, further analysis of the data is needed to fully understand this. The two datasets for 3 mm droplets are very similar, as are those for 3.8 mm droplets. This is due to the initial stages of crater propagation being remarkably similar for the different Weber numbers; the two datasets are virtually indistinguishable

until $t = 0.025$, where the effects of the increased contact area of the droplets with higher Weber numbers for each diameter are becoming evident. The temperature-time profiles get closer to $T^* = 1$ for the higher Weber numbers and it is suggested that this is due to increased heat transfer through their larger contact areas (larger crater surface area). The figure also shows that the larger droplets take longer to heat up to film temperature than their smaller counterparts despite their higher Weber numbers as shown by the lower slope of curve in the low time region of the graph. It is suggested that this may be due to the relationship between crater size and droplet volume meaning that the layer of droplet material on the inside of the crater is thicker and therefore takes longer to reach film temperature.

CONCLUSIONS

This work has determined that established transitions between impingement outcomes upon static films can be applied for impingements on supercritical moving films, if the resultant velocity magnitude is used in place of the normal velocity component. It is noted that some instances of splashing were observed below the expected threshold, but closer examination suggested these were usually due to *prompt* splashing rather than *crown* splashing.

When considering crater evolution and crater morphology, the model for crater radius from Bisighini et al [24] can be applied to the initial stages of crater formation. The craters formed are not hemispherical and so an equivalent radius must be calculated from the area. The normal droplet velocity component (v_n) was found to be the most appropriate to use in the calculations. When viewed from above, the craters formed are not perfectly circular, but distorted slightly to form an elliptical shape, with the major axis of the ellipse being in the flow direction.

The crater shape, when viewed from the side, is observed to develop in line with existing descriptions for static films, however initially it shows some distortion, with the downstream side being slightly deeper than the upstream side, however this distortion is minimal in the later stages of propagation, until the crater is fully formed and begins to recede, with an asymmetry causing the upstream side of the crater to be larger. Any jetting behaviour observed was found to tend downstream, in agreement with the findings of Alghoul et al [1].

When considering the thermal behaviour of droplet-film impacts where the droplet is initially at a different temperature to the film, the data so far obtained shows that the film properties have only a minor effect on the heat transfer with faster, thinner films having a marginally faster heat transfer rate. Droplet Weber number had a more significant effect, with droplets with a higher Weber number heating to film temperature slightly more quickly. However the most noticeable changes were observed when the droplet size was changed, with larger droplets heating more slowly than faster droplets.

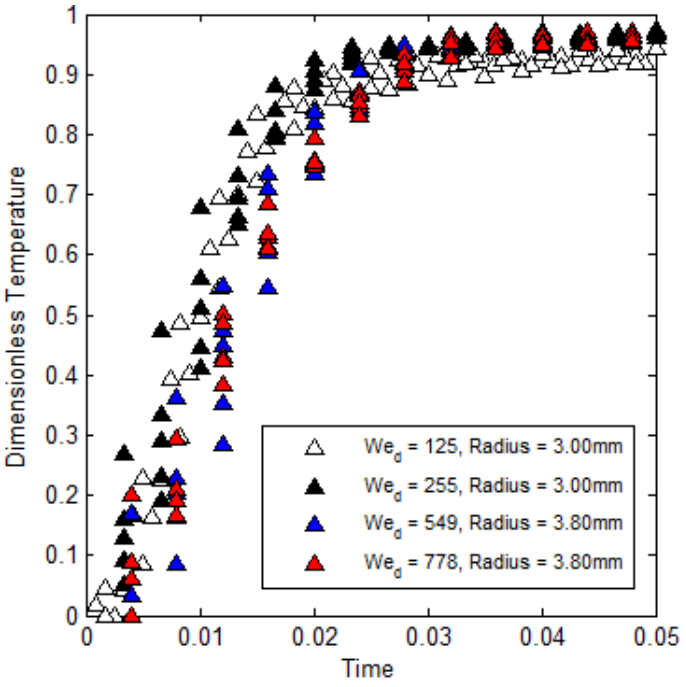

FIGURE 11: **Mean dimensionless temperature against time, obtained from the infrared data**

ACKNOWLEDGEMENTS

We are very grateful for funding for this work from the UK government through an EPSRC ICASE award and from Rolls-Royce plc.

NOMENCLATURE

h_f Film thickness
v_f Film velocity
v_d Droplet velocity
v_n Component of droplet velocity normal to film
g gravitational acceleration
K Splashing parameter
$K_{Cossali}$ Splashing parameter of Cossali, $K_{Cossali} = Oh\, We^{-0.4}$
t Time
$\bar{T}$ Image mean temperature
$\bar{T}_c$ crater mean temperature
T^* Non-dimensional temperature, $T^* = \frac{\bar{T}_c - T_d}{T_f - T_d}$
T_d Droplet temperature
T_f Film temperature
δ Non-dimensional film thickness, $\delta = h_f/\phi$
μ Film liquid viscosity

ϕ Droplet diameter
ρ Film liquid density
σ Film liquid surface tension
σ_T Standard deviation of $\bar{T}$
τ Non-dimensional time, $\tau = \frac{t\phi}{v_n}$
Fr Froude Number, $Fr = \sqrt{\frac{v_f g}{h_f}}$
Oh Ohnesorge Number, $Oh = \frac{\sqrt{We}}{Re} = \frac{\mu}{\sqrt{\rho\sigma\phi}}$
Re Film Reynolds number, $Re = \frac{\rho v_f h_f}{\mu}$
We Droplet Weber number, $We = \frac{\rho\phi^2 v_d}{\sigma}$

REFERENCES

[1] Alghoul, S. K., Eastwick, C. N., and Hann, D. B., 2011. "Normal droplet impact on horizontal moving films: an investigation of impact behaviour and regimes". *Experiments in Fluids,* ***50***(5), pp. 1305–1316.

[2] Worthington, A. "A study of splashes.". *Green, London*.

[3] Coghe, A., Cossali, G., and Marengo, M., 1995. "A first study about single drop impingement on thin liquid film in a low laplace number range". In Proc PARTEC, Vol. 95.

[4] Cossali, G. E., Coghe, A., and Marengo, M., 1997. "The impact of a single drop on a wetted solid surface". *Experiments in Fluids,* ***22***(6), pp. 463–472.

[5] Rein, M., 1996. "The transitional regime between coalescing and splashing drops". *Journal of Fluid Mechanics,* ***306***, pp. 145–165.

[6] Manzello, S., and Yang, J., 2002. "An experimental study of a water droplet impinging on a liquid surface". *Experiments in fluids,* ***32***(5), pp. 580–589.

[7] Manzello, S. L., Yang, J. C., and Cleary, T. G., 2003. "On the interaction of a liquid droplet with a pool of hot cooking oil". *Fire safety journal,* ***38***(7), pp. 651–659.

[8] Manzello, S. L., and Yang, J. C., 2003. "The influence of liquid pool temperature on the critical impact weber number for splashing". *Physics of Fluids (1994-present),* ***15***(1), pp. 257–260.

[9] Manzello, S., and Yang, J., 2002. "An experimental study of a water droplet impinging on a liquid surface". *Experiments in fluids,* ***32***(5), pp. 580–589.

[10] Rioboo, R., Bauthier, C., Conti, J., Voue, M., and De Coninck, J., 2003. "Experimental investigation of splash and crown formation during single drop impact on wetted surfaces". *Experiments in fluids,* ***35***(6), pp. 648–652.

[11] Okawa, T., Shiraishi, T., and Mori, T., 2006. "Production of secondary drops during the single water drop impact onto a plane water surface". *Experiments in fluids,* ***41***(6), pp. 965–974.

[12] Vander Wal, R., Berger, G., and Mozes, S., 2006. "The splash/non-splash boundary upon a dry surface and thin fluid film". *Experiments in Fluids,* ***40***(1), pp. 53–59.

[13] Yarin, A., 2006. "Drop impact dynamics: splashing, spreading, receding, bouncing". *Annu. Rev. Fluid Mech.,* ***38***, pp. 159–192.

[14] Vander Wal, R. L., Berger, G. M., and Mozes, S. D., 2006. "Droplets splashing upon films of the same fluid of various depths". *Experiments in fluids,* ***40***(1), pp. 33–52.

[15] Macklin, W., and Hobbs, P., 1969. "Subsurface phenomena and the splashing of drops on shallow liquids". *Science,* ***166***(3901), pp. 107–108.

[16] Macklin, W., and Metaxas, G., 1976. "Splashing of drops on liquid layers". *Journal of applied physics,* ***47***(9), pp. 3963–3970.

[17] Levin, Z., and Hobbs, P. V., 1971. "Splashing of water drops on solid and wetted surfaces - hydrodynamics and charge separation". *Philosophical Transactions of the Royal Society of London Series a-Mathematical and Physical Sciences,* ***269***(1200), p. 555.

[18] Yarin, A., and Weiss, D., 1995. "Impact of drops on solid surfaces: self-similar capillary waves, and splashing as a new type of kinematic discontinuity". *Journal of Fluid Mechanics,* ***283***(1), pp. 141–173.

[19] Mundo, C., Sommerfeld, M., and Tropea, C., 1995. "Droplet-wall collisions: experimental studies of the deformation and breakup process". *International journal of multiphase flow,* ***21***(2), pp. 151–173.

[20] Huang, Q., and Zhang, H., 2008. "A study of different fluid droplets impacting on a liquid film". *Petroleum science,* ***5***(1), pp. 62–66.

[21] Tropea, C., and Marengo, M., 1999. "The impact of drops on walls and films". *Multiphase Science and Technology,* ***11***(1).

[22] Okawa, T., Shiraishi, T., and Mori, T., 2008. "Effect of impingement angle on the outcome of single water drop impact onto a plane water surface". *Experiments in Fluids,* ***44***(2), pp. 331–339.

[23] Berberović, E., van Hinsberg, N. P., Jakirlić, S., Roisman, I. V., and Tropea, C., 2009. "Drop impact onto a liquid layer of finite thickness: dynamics of the cavity evolution.". *Physical Review E*(79), p. 036306.

[24] Bisighini, A., Cossali, G. E., Tropea, C., and Roisman, I. V., 2010. "Crater evolution after the impact of a drop onto a semi-infinite liquid target". *Physical Review E,* ***82***(3), p. 036319.

[25] Lagubeau, G., Fontelos, M. A., Josserand, C., Maurel, A., Pagneux, V., and Petitjeans, P., 2012. "Spreading dynamics of drop impacts". *Journal of Fluid Mechanics,* ***713***, pp. 50–60.

[26] Šikalo, Š., Tropea, C., and Ganić, E., 2005. "Impact of droplets onto inclined surfaces". *Journal of colloid and interface science,* ***286***(2), pp. 661–669.